J. Biochem. 2009;146(4)549–562
doi:10.1093/jb/mvp100

Structural Insights into the Enzymatic Mechanism of Serine Palmitoyltransferase from *Sphingobacterium multivorum*

Hiroko Ikushiro[1,*], Mohammad Mainul Islam[1,2], Akihiro Okamoto[1,3], Jun Hoseki[1,4], Takeshi Murakawa[1], Shigeru Fujii[5], Ikuko Miyahara[6] and Hideyuki Hayashi[1,†]

[1]Department of Biochemistry, Osaka Medical College, Takatsuki, Osaka 569-8686, Japan; [2]Department of Biochemistry, Wake Forest University School of Medicine, Winston-Salem, NC 27157, USA; [3]School of High Technology for Human Welfare, Tokai University, Numazu, Shizuoka 410-0395; [4]Department of Molecular and Cellular Biology, Institute for Frontier Medical Sciences, Kyoto University, Shogoin Kawahara-cho, Sakyo-ku, Kyoto 606-8507; [5]Laboratory of Chemistry, Kansai Medical University, Hirakata, Osaka 573-1136; and [6]Department of Chemistry, Graduate School of Science, Osaka City University, Osaka 558-8585, Japan

Received May 26, 2009; accepted June 19, 2009; published online June 29, 2009

Serine palmitoyltransferase (SPT) is a key enzyme of sphingolipid biosynthesis and catalyses the pyridoxal 5′-phosphate (PLP)-dependent decarboxylative condensation reaction of L-serine with palmitoyl-CoA to generate 3-ketodihydrosphingosine. The crystal structure of SPT from *Sphingobacterium multivorum* GTC97 complexed with L-serine was determined at 2.3 Å resolution. The electron density map showed the Schiff base formation between L-serine and PLP in the crystal. Because of the hydrogen bond formation with His138, the orientation of the Cα–H bond of the PLP–L-serine aldimine was not perpendicular to the PLP–Schiff base plane. This conformation is unfavourable for the α-proton abstraction by Lys244 and the reaction is expected to stop at the PLP–L-serine aldimine. Structural modelling of the following intermediates indicated that His138 changes its hydrogen bond partner from the carboxyl group of L-serine to the carbonyl group of palmitoyl-CoA upon the binding of palmitoyl-CoA, making the L-serine Cα–H bond perpendicular to the PLP–Schiff base plane. These crystal and model structures well explained the observations on bacterial SPTs that the α-deprotonation of L-serine occurs only in the presence of palmitoyl-CoA. This study provides the structural evidence that directly supports our proposed mechanism of the substrate synergism in the SPT reaction.

Key words: enzyme reaction mechanism, PLP-dependent enzyme, protein structure, serine palmitoyltransferase, sphingolipid biosynthesis.

Abbreviations: ALAS, 5-aminolevulinic acid synthase; AONS, 8-amino-7-oxononanoate synthase; AON, 8-amino-7-oxononanoate; KBL, 2-amino-3-ketobutyrate CoA ligase; KDS, 3-ketodihydrosphingosine; LCB, long chain base; PLP, pyridoxal 5′-phosphate; POAS, PLP-dependent α-oxamine synthase; SPT, serine palmitoyltransferase; spSPT, *Sphingomonas paucimobilis* SPT; smSPT, *Sphingobacterium multivorum* SPT.

Sphingolipids, like glycerophospholipids, are ubiquitous membrane lipids in eukaryotes and some types of bacteria, and are essential for cell survival. It is well known that ceramides play an essential role in structuring and maintaining the water permeability barrier in the skin (*1*). In addition to ceramides, sphingolipid metabolites, such as sphingosine and sphingosine 1-phosphate, are known as the intercellular or intracellular lipid mediators responsible for various cell functions including proliferation, differentiation, apoptosis and stress responses (*2*, *3*). In the plasma membrane, sphingomyelin and sphingoglycolipids are major constituents of the microdomain called 'lipid raft' along with cholesterol, and function as platforms for signal transduction and as the site of the various material transfers via membrane trafficking (*4*).

The biosynthesis of sphingolipids starts by decarboxylative condensation between L-serine and palmitoyl-CoA to generate 3-ketodihydrosphingosine (KDS). The backbone structure of all sphingolipids called the long-chain base (LCB) is formed by this reaction. This reaction is the rate-limiting step of the biosynthetic pathway, and is catalysed by the pyridoxal 5′-phosphate (PLP)-dependent enzyme, serine palmitoyltransferase (SPT) (*5*). In eukaryotes, three kinds of SPT-related genes, SPTLC1 (*Sptlc*1, LCB1), SPTLC2 (*Sptlc*2, LCB2) and SPTLC3 have already been identified (*5–12*). The basic structural unit of mammalian SPTs is a membrane-bound heterodimer, SPTLC1–SPTLC2 or SPTLC1–SPTLC3. SPTLC1 is a common subunit lacking the PLP-binding motif and forms a heterodimer with SPTLC2 or SPTLC3, both of which carries a lysine residue that forms the Schiff base with PLP (*6*, *12*). An octameric model of SPT formed from four SPTLC1–SPTLC2 or SPTLC1–SPTLC3 dimers has been proposed, in which the ratio of the two dimers is

*To whom correspondence should be addressed. Tel: +81-72-684-7291, Fax: +81-72-684-6516,
E-mail: ikushiro@art.osaka-med.ac.jp
†Correspondence may also be addressed. Tel: +81-72-684-6416, Fax: +81-72-684-6516, E-mail: hayashi@art.osaka-med.ac.jp

thought to vary among tissues (*13*). However, further structural/functional analyses of eukaryotic SPTs have been severely hampered by their difficult material preparation arising from the instability and the hydrophobic nature of these SPTs. In contrast to the eukaryotic SPTs, bacterial SPTs function as a water-soluble homodimer and therefore can be easily overexpressed in *Escherichia coli* (*14*, *15*). Bacterial SPTs are highly homologous to each subunit of the eukaryotic SPTs, and are considered to be the prototype of the eukaryotic membrane-bound hetero-oligomeric enzymes. The amino acid residues assumed to be involved in catalysis are conserved between the bacterial SPTs and SPTLC2/SPTLC3.

We have carried out detailed mechanistic studies of the SPT catalytic reaction using the enzyme from *Sphingomonas paucimobilis* EY2395^{T} (spSPT) (*15–20*). Based on the analysis of the reaction with a series of analogues of the amino acid substrate L-serine, it was indicated that the α-carboxyl group of L-serine was crucial for substrate recognition by SPT (*18*). We have synthesized *S*-(2-oxoheptadecyl)-CoA, a non-reactive analogue of the second substrate palmitoyl-CoA, and have made a detailed analysis of the reaction of the SPT–L-serine complex and *S*-(2-oxoheptadecyl)-CoA (*19*). The rate of α-deprotonation of the SPT–L-serine external aldimine intermediate was increased by 100-fold upon the binding of *S*-(2-oxoheptadecyl)-CoA to the enzyme. Accordingly, it was demonstrated that the α-deprotonation of the SPT–L-serine external aldimine intermediate does occur before the Claisen-type C–C bond formation between L-serine and palmitoyl-CoA and the decarboxylation. Based on the combined results of the model-building studies on both the binary and ternary SPT–substrate complexes and the kinetics of the reaction between the SPT–L-serine complex and *S*-(2-oxoheptadecyl)-CoA, it was strongly suggested that His159 is important as an anchoring residue of the α-carboxylate of the L-serine moiety in the external aldimine (*19*). Finally, the site-directed mutagenesis study on His159 of spSPT indicated the multifunctional role of His159 in the SPT catalysis, *i.e*. His159 controls the reaction pathway by adjusting the conformation of the PLP–L-serine external aldimine to prevent unwanted side reactions, and functions as a catalytic residue that promotes the Claisen-type condensation and the following steps (*20*).

In order to verify the reaction mechanism of SPT mentioned above (Scheme 1), structural information on SPT is required. We have isolated SPTs having different characteristics from various sphingolipid-containing bacteria (*15*), and have been trying to crystallize the purified recombinant SPTs. Among them, *Sphingobacterium multivorum* GTC97 SPT (smSPT) yielded a crystal of the L-serine complex with a quality sufficient for an X-ray crystallographic analysis. We report here the crystal structure of smSPT in complex with L-serine at 2.3 Å, which strongly supports our SPT reaction mechanism.

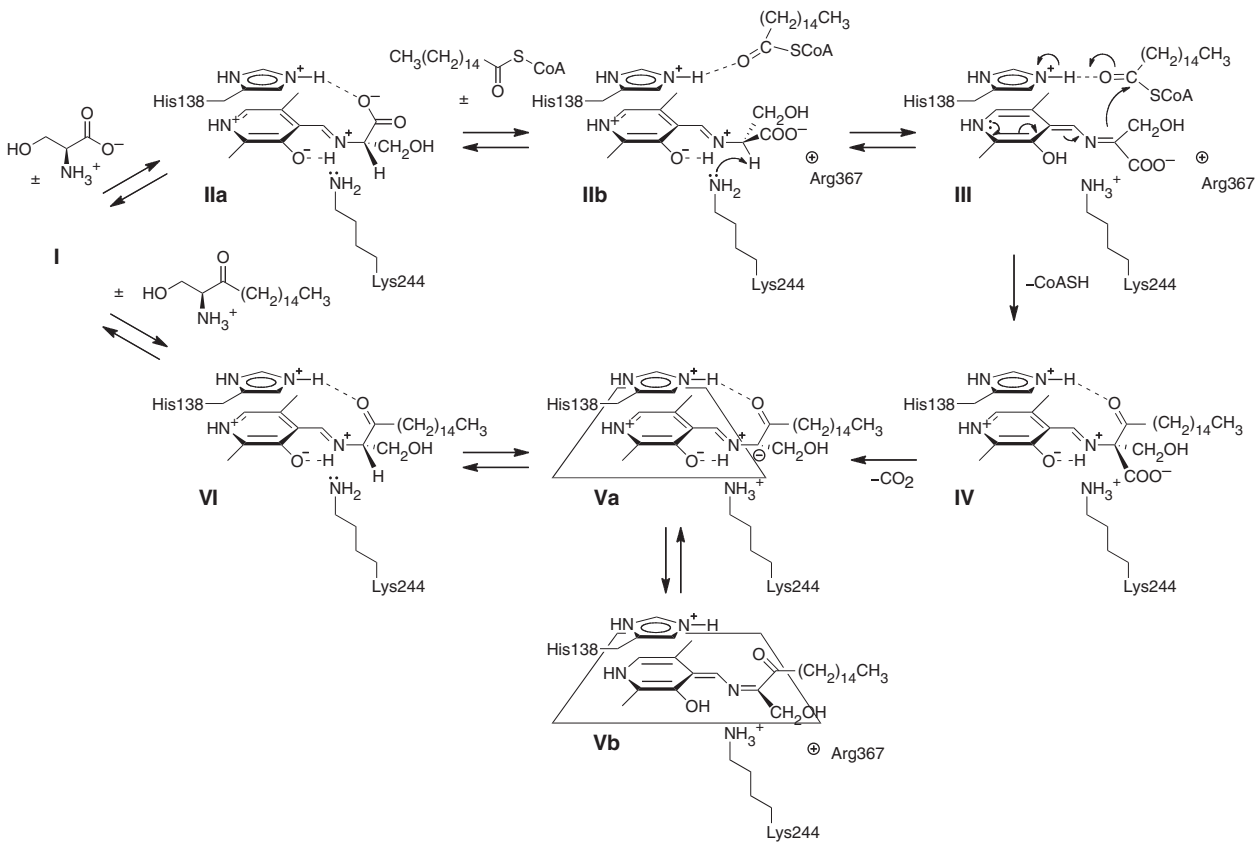

Scheme 1. **Proposed reaction mechanism of SPT.**

EXPERIMENTAL PROCEDURES

Chemicals—Escherichia coli BL21(DE3) pLysS and plasmid pET21b were from Novagen. L-Serine was obtained from Nacalai Tesque (Kyoto, Japan). The PD-10 columns were from Amersham Bioscience/GE Healthcare. All other chemicals were of the highest commercially available grade. S-(2-Oxoheptadecyl)-CoA was synthesized as previously described (*19*).

Expression and Purification of SPT—smSPT was overexpressed in *Escherichia coli* cells and purified as previously described (*15*). The protein concentration of the purified SPT was spectrophotometrically determined using the molar extinction coefficient of $2.68 \times 10^4\,M^{-1}\,cm^{-1}$ at 280 nm for the PLP form of the enzyme (*15*). SDS–PAGE was carried out using the SDS–Tris system with 10% polyacrylamide gel according to the procedure described by Laemmli (*21*).

Spectrometric Measurements—The absorption spectra of SPT were recorded by a Hitachi U-3300 spectrophotometer at 25°C. The CD spectra of SPT were recorded using a Jasco spectropolarimeter J720-WI at 25°C. The buffer solution for the spectrometric measurements contained 50 mM HEPES–NaOH (pH 7.7), 150 mM KCl and 0.1 mM EDTA. SPT was equilibrated with this buffer by gel filtration using a PD-10 (Sephadex G-25) column prior to the measurements.

NMR Samples and Spectral Measurements—For the NMR spectroscopy, all exchangeable hydrogens of the enzyme, the ligands and the buffer base were replaced with deuterium by a previously described method (*19*). Potassium pyrophosphate buffer (50 mM, pH 7.7) prepared in D_2O was used. The ^1H NMR spectra were measured in Wilmad 5-mm NMR tubes kept at 23°C using a Varian UNITY 400 spectrometer operating at 400 MHz. A flip angle of 20° with a relaxation delay time of 5 s was used. To obtain a better signal-to-noise ratio, an exponential window function for 0.2 Hz or 0.5 Hz line-broadening factor was applied to the free induction decays of NMR measurements. Chemical shifts are expressed as p.p.m. relative to an external standard of 3-(trimethylsilyl) propionic acid-d_4.

Crystallization—smSPT was crystallized by the sitting drop vapor diffusion method. A 2 μl aliquot of protein solution (20 mg/ml SPT, 20 mM potasium phosphate pH 7.7, 10 μM PLP) was diluted 2-fold with a reservoir solution (100 mM Tris–HCl pH 8.5, 200 mM sodium acetate, 21.6%(w/v) polyethylene glycol 4000). The droplets were equilibrated against 0.5 ml of the reservoir solution at 20°C. The thin plate-shaped crystals suitable for the X-ray diffraction studies were grown for 2 weeks.

Data Collection—X-ray data from the single crystal was collected at the synchrotron beamline BL38B1 in SPring-8 (Hyogo). The crystal was transferred to a cryo-protectant solution consisting of an 80% reservoir solution [24%(w/v) polyethylene glycol 4000] containing 100 mM L-serine and 20% glycerol, and was rapidly frozen by a cold nitrogen stream at 100 K. The diffraction data were collected on a CCD detector Quantum 4R (Area Detector System Corporation) using a wavelength of 1.0 Å, up to a resolution of 2.3 Å. The X-ray data set was processed by HKL2000 (*22*). The crystallographic data and the processing statistics are summarized in Table 1.

Table 1. **X-ray data collection and refinement statistics.**

Data collection	
Space group	$P4_12_12$
Unit cell dimensions (Å)	
a	61.67
b	61.67
c	207.76
Resolution range (Å)	50–2.3 (2.38–2.3)
No. of reflections	358,532
No. of unique reflections	18,678 (1,796)
Completeness (%)	99.3 (97.7)
R_{merge} (%)	5.8 (10.3)
I/σ (I)	30 (17)
Refinement statistics	
Resolution range (Å)	20–2.3 (2.44–2.3)
No. of reflections (working set)	17,642 (2838)
No. of reflections (test set)	951 (149)
Completeness (%)	99.6 (99.2)
$R_{working}$ (%)	21.2 (23.3)
R_{free} (%)	27.1 (31.6)
No. of protein atoms	3019
No. of co-factor atoms	15
No. of substrate atoms	7
No. of solvent atoms	285
RMSDs from ideal values	
Bond lengths (Å)	0.006
Bond angles (°)	1.2

Values in parenthesis are data for the highest resolution shell.

Structure Determination and Refinement—The smSPT structure was solved by molecular replacement using the program MOLREP (*23*) in the CCP4 suite (*24*). The initial search model of smSPT was built from the structure of the subunit A of 2-amino-3-ketobutyrate CoA ligase (KBL) (PDB entry 1FC4) (*25*) by a homology modeling method using the program MODELLER (*26*). Both space groups, $P4_12_12$ and $P4_32_12$, were used for the searching. The structure of the best solution of the searching with the space groups $P4_12_12$ was well packed around the crystallographic 2-fold axis in the crystal. The unit cell dimension was $a = b = 61.67$ Å, $c = 207.76$ Å. Assuming one subunit per asymmetric unit, V_m was calculated to be 2.3 $Å^3$/Da. Refinement was performed by the program CNS (*27*). Manual rebuilding of the model was carried out by the program XTALVIEW (*28*) based on the composite omit maps calculated by the program CNS and simple omit map. The final model quality was checked with PROCHECK (*29*) and the refinement statistics are summarized in Table 1. The atomic coordinates and structure factors reported here in this article have been deposited in the Protein Data Bank under the accession number 3A2B.

Modelling of Reaction Intermediates of S. multivorum SPT—The modelling of the reaction intermediates of smSPT based on the crystal structure of the PLP–L-serine binary complex was carried out using MOE

(Version 2007.09, Chemical Computing Group, Montréal, Canada) according to the manufacturer's instructions. The initial structure of the substrate-free form of smSPT was constructed using the crystal structure of the internal aldimine of spSPT (Protein Data Bank code 2JG2) (*30*). The crystal structures of both bacterial SPTs were superimposed. The side chain of Lys244 of smSPT was replaced by the PLP–Lys265 aldimine of spSPT, after which the spSPT was deleted. For modelling of the palmitoyl-CoA in the active site of SPT, the crystal structure of *Rhodobacter capsulatus* 5-aminolevulinic acid synthase (ALAS) in a complex with succinyl-CoA (Protein Data Bank code 2BWO) (*31*) was used as the starting structure. The crystal structure of ALAS (subunit D and E) was superimposed on the crystal structure of smSPT, and by subtracting the ALAS protein and PLP, succinyl-CoA was incorporated into the smSPT structure. The carboxyl group of succinyl-CoA was changed to a methyl group and the acyl chain was elongated to C16 using the Molecular Builder of MOE. The water molecules sterically hindering the elongation of the acyl chain were deleted. For the quinonoid intermediate model, the Cα-and Nα-protons of the PLP–L-serine aldimine were deleted. The O-3′ of the quinonoid intermediate was protonated. The bonds at the C2–C3, C5–C6, C4–C4′, and C4′–Cα positions of the PLP–L-serine aldimine were made double bonds. The C3–C4–C4′–Nα dihedral angle of the PLP–L-serine quinonoid was set to 180°. Three water molecules between the carboxyl group of L-serine and Arg-367 were deleted. For the model of the intermediate **IV**, the single bond between Cα of the L-serine and C1 of the palmitoyl-CoA was introduced into the model structure of the ternary complex (intermediate **IIb)** and the CoA moiety was deleted using the Molecular Builder of MOE. For the model of the SPT–KDS complex (intermediate **VI**), the starting structure was made by deleting the carboxylate group derived from L-serine of the intermediate **IV**. As the alternative approach to modeling of the SPT–KDS complex, the crystal structure of *E. coli* 8-amino-7-oxononanoate synthase (AONS) complexed with the reaction product, 8-amino-7-oxononanoate (AON) (Protein Data Bank code IDJ9) (*32*), was used to generate the starting structure. The crystal structure of AONS was superimposed on the crystal structure of smSPT, and AON was incorporated into the smSPT structure by subtracting the AONS protein and the PLP–L-serine aldimine of smSPT. The carboxyl group of AON was changed to a methyl group and the acyl chain was elongated to C16 using the Molecular Builder of MOE. The water molecules sterically hindering the elongation of the acyl chain were deleted. In all cases, protons were generated on the entire structure including the water molecules. Energy minimization was carried out using the MMFF94x force field with all the atoms of smSPT and the ligands allowed to move.

RESULTS

Spectroscopic Properties of smSPT on the Reaction with L-Serine or S-(2-oxoheptadecyl)-CoA—The absorption spectrum of the smSPT is characteristic of the PLP-dependent enzyme with a single peak at 426 nm, which arises from the ketoenamine form of the internal aldimine (PLP–Lys244 Schiff base), in addition to the protein absorption peak at 278 nm (Fig. 1A, *line 1*). The addition of L-serine to the enzyme gave rise to an increase in the intensity of the absorption band with a slight shift to 423 nm (Fig. 1A, *lines 2–9*). These spectral changes showed a hyperbolic dependency on the concentrations of L-serine, and the apparent dissociation constants (K_d) for L-serine were calculated to be 0.47 mM (Fig. 1B). The CD spectrum of the substrate-free form of smSPT showed a positive band at 426 nm, corresponding to the absorption peak (Fig. 1C, *line 1*). In the presence of a saturating amount of L-serine, the CD spectrum exhibited a reversed Cotton effect (Fig. 1C, *line 2*). These results indicated that the transaldimination from the internal aldimine to the external aldimine (PLP–L-serine Schiff base) took place (Scheme 1, **I** → **IIa**). *S*-(2-oxoheptadecyl)-CoA is a nonreactive analogue of the second substrate, palmitoyl-CoA, in which the methylene bridge was introduced between the acyl carbonyl and the CoA sulfur (*19*). When *S*-(2-oxoheptadecyl)-CoA is added to smSPT in the presence of a saturating concentration of L-serine, the 260-nm absorption band derived from the CoA moiety of the analogue increased, but the intensity of the 426-nm peak did not change at all and no absorption peak at around 500 nm corresponding to the quinoniod intermediate was detected (Fig. 1D). These results suggest that *S*-(2-oxoheptadecyl)-CoA does not cause the formation of the quinonoid intermediate of smSPT or that the amount of the quinonoid intermediate formed during the smSPT catalytic reaction is too low to be spectroscopically detected.

S-(2-Oxoheptadecyl)-CoA Enhances the Exchange Rate of the α-Proton of L-Serine by smSPT—The extent of the smSPT-catalysed hydrogen–deuterium exchange at Cα of L-serine was examined by ^{1}H-NMR. In D_2O buffer at pH 7.7, L-serine gives four resonance peaks centered at 3.85 p.p.m. and eight resonance peaks around 3.98 p.p.m., corresponding, respectively, to the α- and the β-protons. Although the spectrum was almost unchanged when only SPT was added to the solution, the further addition of *S*-(2-oxoheptadecyl)-CoA to the solution caused a time-dependent decrease in the α-proton signal without altering the intensity of the β-protons (data not shown). The rate of the hydrogen-deuterium exchange was quantitatively analysed by following the relative intensities of the α/β-protons as shown in Fig. 2. The time-dependent decay of the α-proton signals were well fit to the following single exponential function:

$$y = A \cdot e^{-k_{app}t}$$

where A is the initial value of the α/β ratio (y), usually around 0.485, and k_{app} is the apparent rate constant. No decrease in the α/β ratio was observed in the control experiments (without smSPT). When L-serine was incubated with only smSPT, a very slow exchange of the α-proton of L-serine with $t_{1/2} = 40.44 \pm 0.61$ h was observed, indicating that the α-deprotonation slowly proceeds in the external aldimine. On the other hand, when *S*-(2-oxoheptadecyl)-CoA was added to the reaction

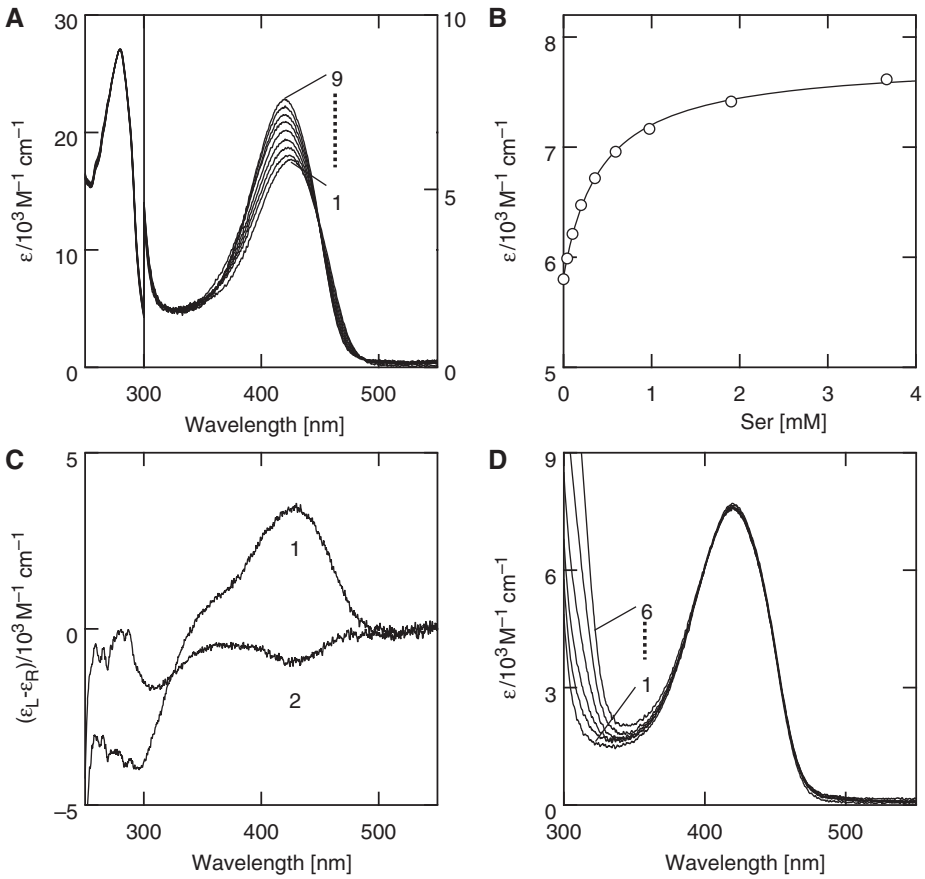

Fig. 1. **Absorption and CD spectra of *S. multibvolum* SPT in the presence of L-serine and *S*-(2-oxoheptadecyl)-CoA.** The buffer system was 50 mM HEPES–NaOH (pH 7.7) containing 150 mM KCl and 0.1 mM EDTA. The measurements were done at 25°C. The enzyme concentration was 6.76 μM. (A) Absorption spectra of SPT in the presence of L-serine. Curve line 1 is the spectrum of the substrate-free form of SPT. Curve lines 2–9 are those taken in the presence of 0.04, 0.10, 0.20, 0.36, 0.59, 0.98, 1.90 and 3.67 mM of L-serine, respectively. (B) Titration curve of the molar extinction coefficient at 424 nm versus the L-serine concentration. (C) CD spectra in the absence (Curve line 1) and presence (Curve line 2) of 3.67 mM L-serine. (D) Absorption spectra of SPT in the presence of L-serine and *S*-(2-oxoheptadecyl)-CoA. Curve lines 1–6 are taken in the presence of 5 mM of L-serine and 0, 0.01, 0.05, 0.10, 0.15 and 0.25 mM of *S*-(2-oxoheptadecyl)-CoA, respectively.

solution, the rate of the exchange was apparently increased with $t_{1/2}$ being decreased to 1.30 ± 0.03 h. This clearly shows that *S*-(2-oxoheptadecyl)-CoA binds to the smSPT–external aldimine complex and enhances the α-deprotonation of L-serine in the external aldimine. This is in accordance with the phenomena observed for spSPT (*19*). However, the analogue-induced enhancement of the α-deprotonation was 135-fold for spSPT, whereas the value was 31.1-fold for smSPT. This indicates that the equilibrium between the external aldimine and the quinonoid intermediate (Scheme 1, **IIb** and **III**, respectively) in smSPT slightly shifts to the former as compared to spSPT.

Quality of the Crystal Structure of the smSPT–External Aldimine Complex—The structures of smSPT complexed with the amino acid substrate L-serine was determined by the molecular replacement method using the structure of KBL and refined to a 2.30-Å resolution. The main-chain torsion angles conform to standard values for non-glycine/non-proline residues, with 90.3% falling within the most favored regions of the Ramachandaran plot and 9.2% in the additionally allowed regions as determined by PROCHECK (*29*). The dimer is produced by applying the $(-y, -x, 1/2-z)$ crystallographic symmetry operation of the $P4_12_12$ space group to the monomer in the asymmetric unit. The final model contains 392 amino acid residues, one PLP–L-serine Schiff base (*i.e.* external aldimine) structure and 137 water molecules per monomer, and yield a crystallographic *R*-value of 21.2% and an R_{free}-value of 27.1% with an ideal geometry. The last six C-terminal residues were not visible and therefore the final model contained 392 of 398 amino acids from Ser2 to Ala393. A clear electron density for both the PLP and substrate serine molecules was visible in the omit map as shown in Fig. 3. The results of the refinement are summarized in Table 1.

Overall Structure of the smSPT–External Aldimine Complex—Figure 4 shows the overall structure of the smSPT–external aldimine complex. The smSPT molecule was found as a tightly interacting and interlocked dimer structure in the crystal. The surface area of the subunit interface was calculated to be 17497.6 Å^2, which amounts to about 30% of the subunit surface area. smSPT is structurally classified into the fold type I family of the

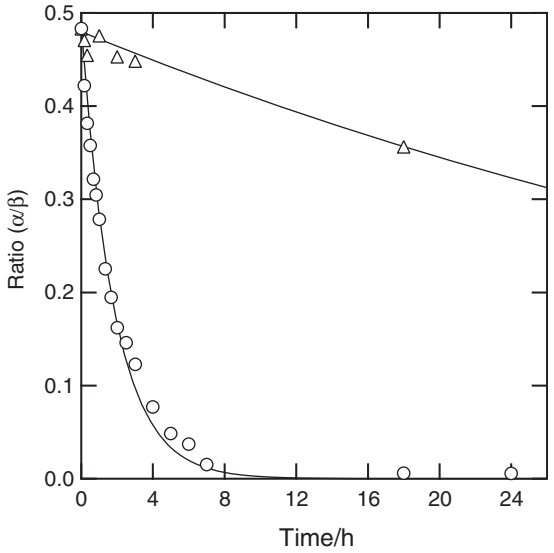

Fig. 2. **Time course of the hydrogen–deuterium exchange at the α-C of L-serine.** The hydrogen–deuterium exchange at the α-C of 10 mM L-serine was followed by ^{1}H-NMR in the presence of 5 μM SPT. The hydrogen–deuterium exchange reaction at Cα of L-serine by the SPT decreased the intensity of the α-proton peak and changed the splitting of the β-methylene protons from octet to quartet without changing the integrated intensity of the β-methylene protons. The ratios of the integrated intensity of the α-proton to that of the β-protons are plotted versus the reaction time. The lines represent theoretical fits to a single-exponential decay equation ($y = A\exp^{-K_{app}t}$). Open circle; 10 mM L-serine was incubated with 5 μM SPT and 1.5 mM *S*-(2-oxoheptadecyl)-CoA, open triangle; 10 mM L-serine was incubated with 5 μM SPT.

PLP-dependent enzymes for which aspartate aminotransferase is the prototype (*33–36*). Each monomer can be divided into three segments, an N-terminal domain comprising residues 2–23, a small domain formed by two parts of the polypeptide chain from residues 24–59 and 295–393, and a large domain from residues 60–294. The N-terminal domain consists of two helices, which extends away from the rest of the monomer. The small domain assumes an α/β structure with a spirally twisted, six-stranded-like β-sheet surrounded by three α-helices from the surface side of the small domain. The large domain is also an α/β structure which includes a large, open twisted, seven-stranded β-sheet and ten α-helices. This β-sheet, in which six strands (β3, β8, β7, β6, β4 and β5) are parallel while only β9 is interposed between β3 and β8 as an anti-parallel strand, is characteristic of the fold type I of the PLP enzymes. Many of the active-site residues are situated at or near one end of a seven-stranded β-sheet. All of the three domains of the monomer participate in the dimerization. The suitable assembly of both the large domains and small domain of the monomer makes the substrate-binding pocket with a narrowing and reversed conical shape between them. Therefore, the active site within a monomer is complemented by the amino acid residues from the second monomer. This substrate-binding pocket is connected to the enzyme surface by a channel, which is created by the same domains involved in forming the active site. As previously reported for the substrate-free form of spSPT by Yard *et al*. (*30*), two long hydrophobic channels where the C16 aliphatic acid chain of palmitoyl-CoA could reside were also observed in smSPT. In the smSPT crystal, the water molecules occupy these channels instead of palmitoyl-CoA.

Active Site Structure of smSPT–L-Serine External Aldimine Complex—The residual electron density observed in the active site cavity of SPT in an $F_o - F_c$ omit map fitted well to the cofactor PLP and the substrate L-serine, and the electron density of L-serine is connected to the C4A atom of the PLP indicating that L-serine is covalently bonded to PLP (Fig. 3). The geometry around the Cα atom of the bound L-serine is clearly tetrahedral, showing that the PLP–L-serine complex is the external aldimine, and not the quinonoid intermediate. The Nα = C4A double bond is coplanar with the pyridoxal ring, and the L-serine–PLP complex does not exhibit any significant deviations from the idealized geometry. It is clear from the electron density that there is no covalent linkage between the PLP cofactor and Lys244 (Fig. 3). As shown in Fig. 5B, the side chain of Lys244 is directed away from C4 of PLP, and its ε-amino group forms hydrogen bonds with the side chains of Ser243 and Thr241. The pyridine ring of PLP is stacked between the side chains of His138 and Ala212 by hydrophobic interactions, and is held in position by a hydrogen bond from the side chain of Asp210 to the positively charged nitrogen of PLP (N1) (Fig. 5). The imidazole ring of His138 is situated at the *re* face of PLP and is parallel to the pyridine ring of PLP. The O3 atom of PLP forms a hydrogen bond to Nε2 of His213, which in turn forms a hydrogen bond between its Nδ1 and the Tyr54 hydroxyl group. The phosphate moiety of PLP is anchored by polar interactions with the active site residues, such as the main chain N atoms of Phe114 and Ala274* and the side chains of Ser243 and Ser273*, and two water molecules[1]. The hydroxyl group of L-serine forms hydrogen bonds with the phosphate group of PLP and one water molecule, and indirectly interacts with Ser243 via this water molecule. The carboxyl group of L-serine forms hydrogen bonds with Nε2 of His138 and two water molecules, and indirectly interacts with Ser81*, Met271* and Asn52 via these water molecules. Because of the interaction with His138, the orientation of the carboxyl group of L-serine inclines 80° against the PLP pyridoxal ring.

DISCUSSION

Structure Comparison between spSPT and smSPT—smSPT is very similar to spSPT with a 38% sequence homology (*15*). Recently, the crystal structure of the substrate-free form of spSPT had been determined (*30*). We have not been able to obtain crystals of the substrate-free form of smSPT at present, but have succeeded in determining the crystal structure of the

[1] To distinguish the residues from the two subunits of a biological dimer, we labeled the residues from the opposite subunit with an asterisk.

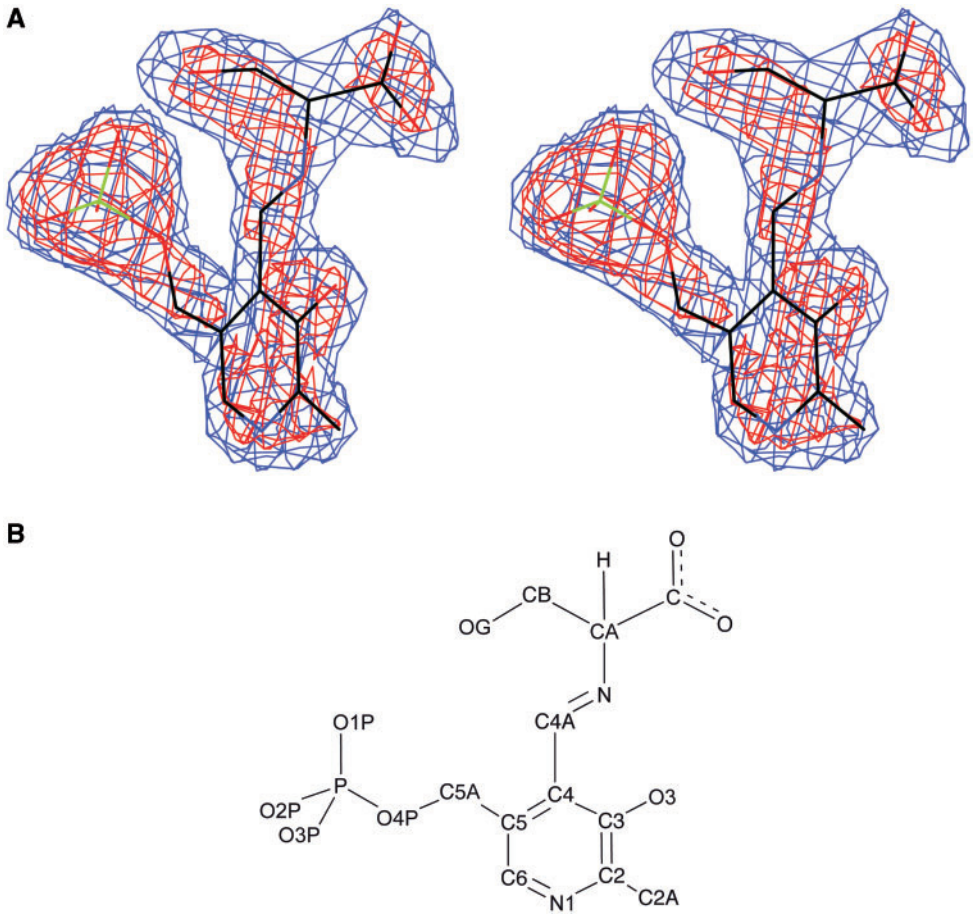

Fig. 3. **Stereo drawing of omit map for SPT–L-serine external aldimine.** (A) Electron density around the PLP-L-serine Schiff base (external aldimine) of SPT. The $F_o - F_c$ omit maps were contoured at the 2.5 σ and 3.5 σ levels and superimposed with the final refined model. (B) The chemical structure of the PLP-L-serine Schiff base.

amino-acid-substrate bound form of the enzyme. The observed residual electron density in the active site cavity of SPT clearly matched well with the PLP Schiff base with the substrate L-serine, but not the PLP Schiff base with Tris, which was used as the buffer base for crystallization (Fig. 3). Based on the dissociation constant (K_d) values of smSPT for L-serine (0.47 mM) and Tris (38 mM), L-serine should preferentially bind to smSPT during crystallization in the solution containing 80 mM of each compound.

The structure alignment of smSPT and spSPT showed that the region from Gly4 to Ala393 of smSPT corresponds to that from Arg22 to Val416 of spSPT (2JG2), except for five insertions, Ile32, Thr44, Lys55, Glu343 and Thr344 in spSPT. There is no significant difference in the overall structure of both enzymes; the RMSD value for the Cα atoms of the two structures in the 390 amino acid residue region is 1.42 Å. Specifically, the Pro379–Pro380 peptide bond of spSPT adopts a *cis* conformation, and Ser356–Pro357 of smSPT also adopts the same conformation. The minute differences between the two SPT structures are as follows: While the N-terminal region from Arg22 to Ser41 is the 1st α-helix in spSPT, the N-terminal region of smSPT bends to form two α-helices (Lys3–Gln12 and Lys14–Lys22) due to the deletion of the amino acid residue corresponding to Ile32 of spSPT. The β-sheet composed of three β-strands in the N-terminal domain and one β-strand in the small domain of spSPT corresponds to the β-sheet formed by three β-strands in the small domain of smSPT. The deletion of the amino acid residue corresponding to Lys55 of spSPT results in the lack of the first β-strand in this region of smSPT. In a similar fashion, the core of the small domain of smSPT, where the residues corresponding to Arg339–Lys340 of spSPT are absent, contains a β-sheet formed by three β-strands. The large domain of smSPT lacks the anti-parallel β-sheet composed of the two β-strands of Val204–Tyr205 and Asp210–Ile211 in spSPT.

The architectures of the active sites of smSPT and spSPT closely resemble each other, although the former is the substrate-free form and the latter, the external aldimine form. The residues of smSPT making contact with the external aldimine, such as Arg367, Asp210, His213 and His138 are almost completely overlapped with those of spSPT with the exceptions of Lys244 (which forms the external Schiff base with L-serine) and Asn52. The Asn residue corresponding to Asn52 of smSPT is conserved among other members of PLP-dependent α-oxamine synthase (POAS) family, and

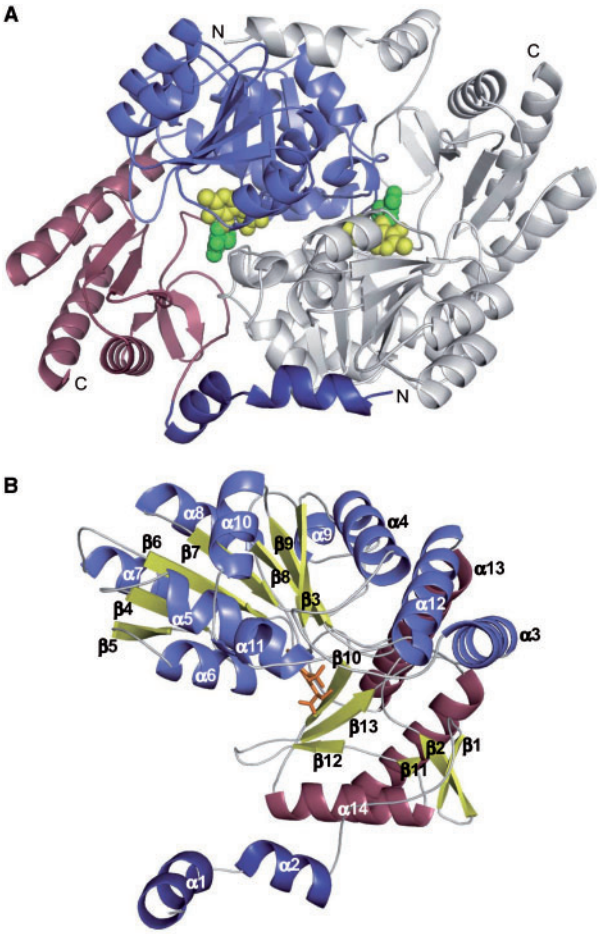

Fig. 4. **Overall structure of the SPT in complex with L-serine.** (A) Ribbon diagram of the SPT symmetric dimer in a complex with L-serine. The three structural domains of subunit A are coloured to highlight the N-terminal domain (*dark blue*), the small domain (*red*) and the large domain (*light blue*), whereas subunit B is shown in *grey*. The N- and C-termini are labelled. The PLP and L-serine in each monomer are shown as *yellow* and *green space-fill* models, respectively. (B) Ribbon diagram of the SPT monomer in a complex with L-serine. The α-helices among the three structural domains of the monomer are colored as the same as panel A, but the β-sheets are in yellow. Secondary structure elements and the N- and C-termini are labelled. The PLP–L-serine aldimine is shown in an *orange-coloured stick* model. The figures were drawn using PyMOL v0.99 (DeLano Scientific).

contributes to the substrate recognition and the catalysis of these enzymes. Asn52 is substituted by Tyr73 in spSPT; a similar substitution by Tyr is also observed in the human SPTLC2 and SPTLC3. The atoms Cγ, Cδ1, Cδ2 of spSPT Tyr73 overlap with Cγ, Oδ1, Nδ2 of smSPT Asn52. In addition, the hydroxyl group of spSPT Tyr73 occupies the same position as the water molecule that lies between Asn52 and Arg367 in smSPT. This accounts for how the bulky Tyr73 side chain is accommodated in the active site of spSPT. Based on the results of the model building study, we have speculated that, in spSPT, Arg390 instead of Tyr73 forms the hydrogen bonds to the carboxylate of L-serine in the ternary complex of SPT–L-serine–palmitoyl-CoA (*19*). As the residue corresponding to Arg367 of smSPT, Arg368 of *E.coli* KBL interacts with the carboxylate group of 2-amino-3-ketobutyrate (*32*), and Arg374 of *R. capsulatus* ALAS interacts with the carboxylate group of glycine together with Asn54 (*31*). In the crystal structure of the *E.coli* AONS–AON complex, Asn47 forming a hydrogen bond with Arg364 was speculated to fix the α-carboxylate of L-alanine during the catalytic cycle (*32*). Combining these observations together, we consider that, in the case of smSPT, Asn52 and Arg367 locating at the suitable position may contribute to the fixation of the carboxylate of L-serine at the later step of the catalytic cycle.

Conserved Hydrogen Bond Network in the Active Site of the α-Oxamine Synthase Family—Although the hydrogen bonds between the active site lysine residue and the PLP phosphate group are observed in the AONS and KBL crystals (*26*, *32*, *37*), Ser243 and the hydroxyl group of the substrate L-serine rather than the Nε of Lys244 are close to the PLP phosphate group and form hydrogen bonds in the smSPT crystal structure (Fig. 5). smSPT completely conserves the hydrogen bond network of Arg367(Nη1)–Ser185(main chain O)–Ser185(main chain N)–water–Asp181(Oδ1)–Asp181(Oδ2)–His138(main chain N)–His138(Nδ1)–Ser140(Oγ), which corresponds to the network reported in the external aldimine structures of AONS–AON and KBL–2-amino-3-ketobutyrate (*26*, *32*). While the keto oxygen and the carboxyl oxygen of 2-amino-3-ketobutyrate form hydrogen bonds to the guanidinium group of Arg368 in KBL, such an interaction between the carboxyl group of L-serine and Arg367 was not observed in the crystal structure of the L-serine external aldimine intermediate of smSPT.

The Orientation of the Carboxyl Group of L-Serine in the Crystal Structure of the smSPT–External Aldimine Complex—For all the PLP-dependent enzymes whose crystal structures have already been elucidated, the expected conformation of the external aldimine (PLP–substrate Schiff base) conforms to Dunathan's conjecture (*38*). This conjecture explains the stereochemical control of the electron sink ability of PLP as follows: the PLP-dependent enzyme places one of the bonds of the substrate Cα perpendicular to the imine–pyridine plane in order to break the bond. Through this conformation of the external aldimine, the developing p-orbital of the substrate Cα during the bond cleavage is aligned so that it has the maximum overlap with the extended π-orbital of the imine–pyridine conjugate system, thereby lowering the energy of the transition state and increasing the reaction rate. Previously, based on the ^{1}H-NMR analyses of the reaction of the spSPT with L-serine, we hypothesized that the conformation of the Cα–H bond of L-serine in the SPT external aldimine would be unfavorable for cleaving the bond (*19*). The following model-building study (*19*) and analysis of the His159 mutant enzymes (*20*) suggested that the strong hydrogen bond formed between His159 and the carboxylate group of the L-serine moiety of the PLP–L-serine aldimine fixes the Cα–H bond in an orientation away from the maximum p–π overlap indicated by Dunathan's conjecture. In accordance with this, the carboxyl group of L-serine

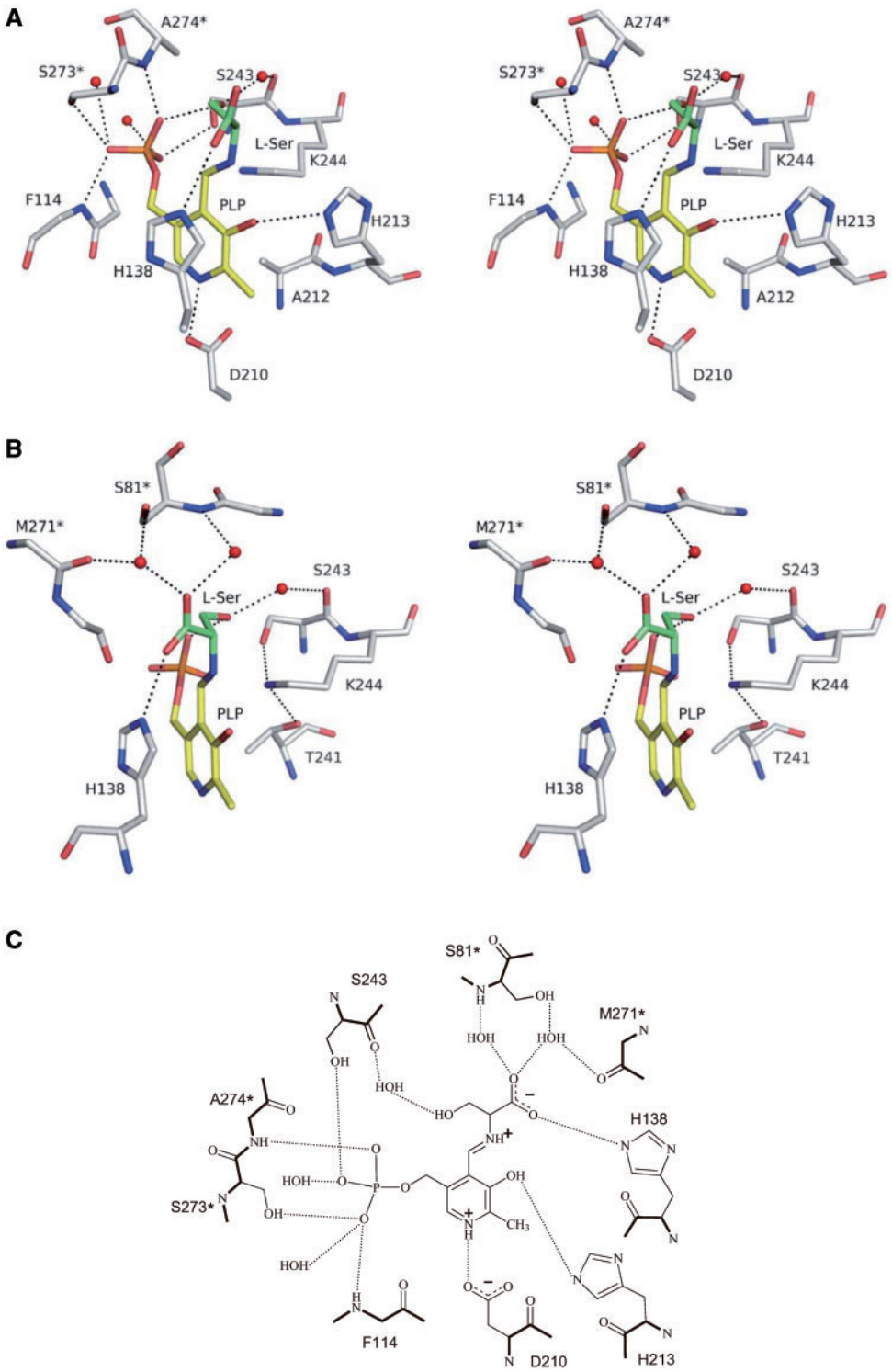

Fig. 5. **The active site of the SPT–L-serine external aldimine complex.** (A) The *stick* model representation of the PLP binding site of SPT. The front of the figure is the solvent side (entrance of the active site). (B) The *stick model* representation of the L-serine binding site of SPT. The left part of the figure is the solvent side (entrance of the active site). The cofactor and L-serine are drawn in *yellow* with *orange* phosphorus and *green*, respectively. The water molecules are depicted as *red* balls. Possible hydrogen-bond pairs are connected by dotted lines. The stereo figures in the parallel view were drawn using PyMOL v0.99 (DeLano Scientific). (C) The schematic drawing of the hydrogen bond network between the PLP–L-serine external aldimine and the amino acid residues of the SPT active site including the water molecules.

takes an almost perpendicular orientation to the imine–pyridine plane and strongly interacts with the Nε2 of His138 in the crystal structure of the smSPT–external aldimine complex (Fig. 5). Through fixation of the carboxyl group, the Cα–H bond of L-serine is only ~24° out of the imine–pyridine plane. This well accounts for the observations on smSPT that the binding of L-serine alone does not cause accumulation of the quinonoid intermediate (Fig. 1) and that the external aldimine exchanges the α-hydrogen with the solvent at a very slow rate (Fig. 2).

Structural Aspects of the Enzymatic Reaction—Based on the crystal structures of the SPT–L-serine external aldimine complex and other members of the POAS family, we have constructed the structure models of the smSPT reaction intermediates as shown in Fig. 6. Combined with our previous kinetic analyses on the wild-type and the mutant SPT, the reaction mechanism of SPT can be discussed as follows. Figure 6A shows a model of the internal aldimine of smSPT (Scheme 1, **I**), which was constructed based on the crystal structure of the substrate-free form of spSPT. As described above, the architectures of spSPT and smSPT closely resemble each other. PLP forms the internal aldimine with the ε-amino group of Lys244. Both Asp210 and His213 are also important for the proper positioning of PLP by the interaction with N1 and O3 in the pyridine ring, respectively. It was also observed that His138 stacks with the PLP pyridine ring. The SPT reaction is initiated by the binding of L-serine to the enzyme, and via subsequent transaldimination assisted by His213, the external aldimine is formed between PLP and the α-amino group of L-serine (Scheme 1, **I** → **IIa**). Figure 6B shows the crystal structure of the external aldimine in the smSPT–L-serine binary complex (Scheme 1, **IIa**). As described in the previous section, the conformation of the external aldimine, which is brought about by the hydrogen bond between L-serine and the Nε2 of His138, is unfavorable for the α-deprotonation of L-serine. To construct the model for the ternary complex of SPT–L-serine–palmitoyl-CoA, the crystal structure of *R. capsulatus* ALAS–succinyl-CoA complex was used because it is the only structure known at present on the POAS family enzyme complexed with acyl-CoA substrate (*31*). The amino acid residues directly interacting with the adenine moiety and the ribose moiety of the succinyl-CoA are almost completely conserved in smSPT, such as Leu133, Asp134, Glu135, His138, Ala139, Ile142 and Lys154, enabling us to incorporate palmitoyl-CoA into the crystal structure of smSPT complexed with L-serine. Energy minimization of the ternary complex model converged into a geometry (Fig. 6C) similar to the corresponding model of spSPT proposed previously (*19*). In this model, the thioester O of palmitoyl-CoA forms a stable hydrogen bond with the Nε2 atom of His138, displacing the carboxylate of L-serine. The carboxylate of L-serine, in turn, formed hydrogen bonds with the guanidinium group of Arg367, and shows a week interaction with the side chain of Asn52. This interaction fixes the PLP–L-serine external aldimine to a new conformation, in which the Cα–H bond is almost perpendicular to the imine–pyridine plane and approaches the ε-amino group of Lys244. Both factors are preferable for the α-deprotonation to proceed (Scheme 1, **IIa** → **IIb**), and this properly explains the acceleration of the α-deprotonation of the external aldimine by *S*-(2-oxoheptadecyl)-CoA (Fig. 2). The model for the quinonoid intermediate was derived from the model for the ternary complex. In this model (Fig. 6D), the hydrogen bonds from the thioester O of palmitoyl-CoA to the Nε2 atom of His138, and the hydrogen bonds/ionic interactions of the L-serine carboxyl group to the side-chains of Arg367 and Asn52 became more stable than those in the ternary complex, due to the planer conformation of the PLP–L-serine quinonoid intermediate. The C–C bond is formed by the Claisen-type condensation reaction between the quinonoid intermediate and palmitoyl-CoA, *i.e*. the nucleophilic attack of the carbanionic Cα of the quinonoid intermediate to the carbonyl C of palmitoyl-CoA (Scheme 1, **III** → **IV**). In this step, His138 may act as an acid catalyst, which donates the proton to the carbonyl oxygen of palmitoyl-CoA and helps with polarization of the carbonyl group. Figure 6E shows the model structure of the intermediate just after the condensation reaction between L-serine and palmitoyl-CoA (Scheme 1, **IV**). After energy minimization, the hydrogen bond between Nε2 of His138 and the carbonyl oxygen derived from palmitoyl-CoA was kept at a distance of 2.41 Å in the model of **IV**. The Cα–COO^- bond of the condensation product was 24° out of the imine–pyridine plane and set at 131° to the plane of the carbonyl group. This indicates that the cleavage of the Cα–COO^- bond would be assisted by the carbonyl group rather than the imine–pyridine conjugate system. The hydrogen bond between the protonated His138 Nε2 and the carboxyl group is expected to polarize the carbonyl group and further assist the decarboxylation. This mechanism has been proposed for ALAS in the condensation reaction of glycine and succinyl-CoA (*39*). After decarboxylation, the hydrogen bond between His138 and the carbonyl group is still retained (Fig. 6F). This structure is analogous to the crystal structure of the AONS–AON complex in which a hydrogen bond is formed between His133 with O7 of AON (*32*). Therefore, we can expect that the role of the conserved His residue as an acid catalyst for the decarboxylation may be common to the POAS family enzymes.

Structural Interpretation for the Differences in the Spectroscopic Properties between spSPT and smSPT—Some differences in the spectroscopic properties between spSPT and smSPT were observed. As is the case for spSPT, the absorption spectrum of smSPT is pH-independent, indicating that the pK_a of the Schiff base nitrogen is high enough to keep it in the protonated state. However, smSPT shows only a single peak at 426 nm derived from PLP (Fig. 1), which is in contrast to spSPT having a large absorption peak at 426 nm (ascribed to the ketoenamine) and a small peak at 338 nm (ascribed to the enolimine). Although we cannot determine what causes the difference without the crystal structure of the substrate free form of smSPT, the tautomeric shift from the ketoenamine form to the enolimine form in smSPT should reflect the microenvironment around O3–Nζ of the PLP internal Schiff base. We had reported that the quinonoid intermediate was stably

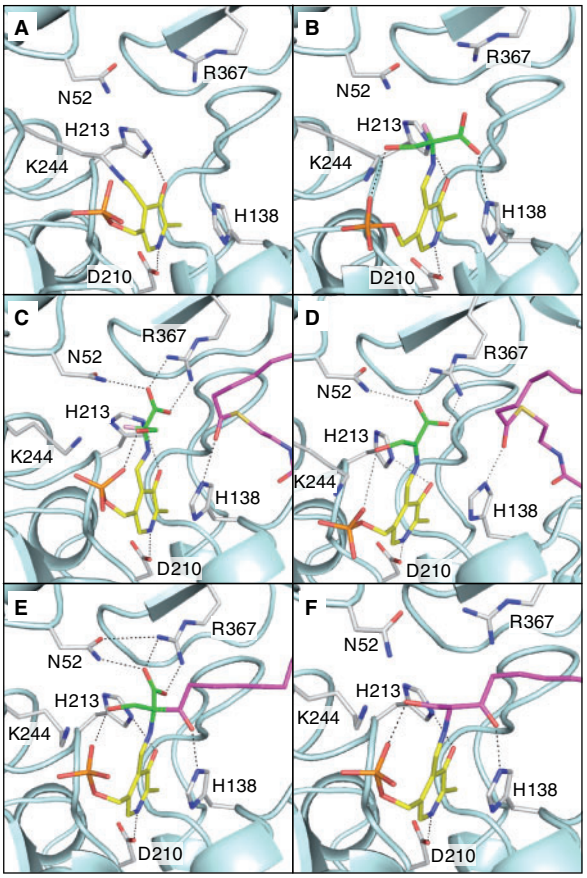

Fig. 6. **Close-up views of SPT catalytic intermediate models and crystal structure.** Modelling of the SPT reaction intermediates based on the crystal structure of the SPT–L-serine external aldimine was carried out using MOE (Version 2007.09, Chemical Computing Group, Montréal, Canada). The SPT monomer is shown in *ribbon* diagram. The catalytic residues, Asn52, His138, Asp210, His213, Lys244 and Arg367 are shown in *stick* diagram. PLP, L-serine, palmitoyl-CoA and KDS are shown as *yellow*, *green*, *magenta* and *purple-coloured sticks*, respectively. (A) Substrate-free form of SPT. Lys244 forms the internal aldimine linkage with PLP. (B) The crystal structure of the external aldimine intermediate in the SPT–L-serine complex. The α-proton of L-serine is highlighted for easy visualization. Because of the fixation of the carboxyl group of L-serine by His138, the α-proton of L-serine is not perpendicular against a PLP-pyridine ring. (C) The external aldimine intermediate in the ternary complex of SPT, L-serine and palmitoyl-CoA. The α-proton of L-serine is highlighted for easy visualization. His138 formed a hydrogen bond with the C1 carbonyl oxygen of palmitoyl-CoA at a distance of 2.71 Å. The carboxyl group of L-serine forms two new hydrogen bonds with the guanidino group of Arg367 and δ-amino group of Asn52 with the distances of 2.33, 2.37 and 2.58Å. The α-proton of L-serine took a perpendicular orientation against the plane formed from the PLP-pyridine ring and the double bond of the Schiff base, suitable for the α-proton abstraction by the Lys244 ε-amino group located at a distance of 3.14 Å. (D) The quinonoid intermediate in the ternary complex of SPT, L-serine and palmitoyl-CoA. A network of protein–PLP–substrate interactions stabilized the planar geometry of the quinonoid intermediate. His138 interacted with the C1 carbonyl oxygen of palmitoyl-CoA at a distance of 2.51 Å. (E) Intermediate IV (see Scheme 1). His138 formed a hydrogen bond with the carbonyl oxygen derived from palmitoyl-CoA at a distance of 2.41 Å. The carboxyl group derived from L-serine formed tight hydrogen bonds with the guanidino group of Arg367 and δ-amino group of Asn52 at the distances of 2.36, 2.38 and 2.58 Å. Cα–COO^- takes a perpendicular conformation to the plane of the carbonyl group, suitable for the subsequent decarboxylation reaction. (F) SPT–KDS complex. His138 formed a hydrogen bond with the C3 keto oxygen of KDS with a distance of 2.41 Å. Panels were drawn using PyMOL v0.99 (DeLano Scientific).

accumulated by the incubation of spSPT with both L-serine and *S*-(2-oxoheptadecyl)-CoA (*19*). Even though the acceleration of the α-deprotonation of L-serine induced by the binding of *S*-(2-oxoheptadecyl)-CoA was also observed for smSPT, the quinonoid intermediate accumulation was not spectroscopically detected (Figs 1D and 2). Based on the crystal structure of the substrate-free form of spSPT, His159 and Arg390 are surely expected to interact with the thioester O of palmitoyl-CoA and the L-serine carboxyl group, respectively. However, contrary to Asn52 of smSPT, Try73 of spSPT is close enough to directly interact with the side chain of Arg390 and the carboxylate group of the substrate L-serine. This bulky hydroxyphenyl group of Try73 may stabilize the quinonoid conformation in the ternary complex, by stacking parallel on the plane formed from the guanidinium group of Arg390 and the carboxyl group of L-serine. Therefore, in the ternary complex, the equilibrium between the external aldimine and the quinonoid may shift to the quinonoid formation.

Speculation about the HSN1-Mutation Based on the Crystal Structure of smSPT—The single mutations (C133W, C133Y, V144D and G387A) in human SPTLC1 cause HSN1, a hereditary disorder of peripheral sensory neurons (*40–42*). The decrease in the sphingolipid synthesis caused by the dominant negative inhibition of the SPT activities has been speculated to be related to the neurodegeneration in HSN1 (*43–45*). Cys133 and Val144 of the human SPTLC1 correspond to Ala79 (or neighboring Cys78) and Ile90, respectively, of smSPT (Fig. 7). These amino acid residues do not directly contact the coenzyme or the substrate but lie at both ends of the loop between helix-3 and helix-4. This loop directly contacts the small domain of the other monomer to maintain the dimer structure, and contains the catalytically important residue Ser81* near the center of the loop that interacts with the carboxylate group of the substrate L-serine via two water molecules. The substitution of Ala79 (or Cys78) by the more bulky Trp and Tyr residues, or the substitution of the non-polar Ile90 by the acidic Asp residue should cause a slight distortion of the main chain at both ends of the loop. This distortion, albeit slight, might induce a large movement in the peptide chain at the center of the loop. Therefore, it is easily expected that the enzymatic activity of SPT would be affected by the HSN1-type mutations via the disorder in the geometry of the key residues in the active site that participates in the substrate recognition, or via the imperfect dimerization of the SPT monomers.

CONCLUSIONS

The crystal structure of smSPT in a complex with the amino acid substrate, L-serine, has been determined at a 2.3 Å resolution. The observed interactions between the

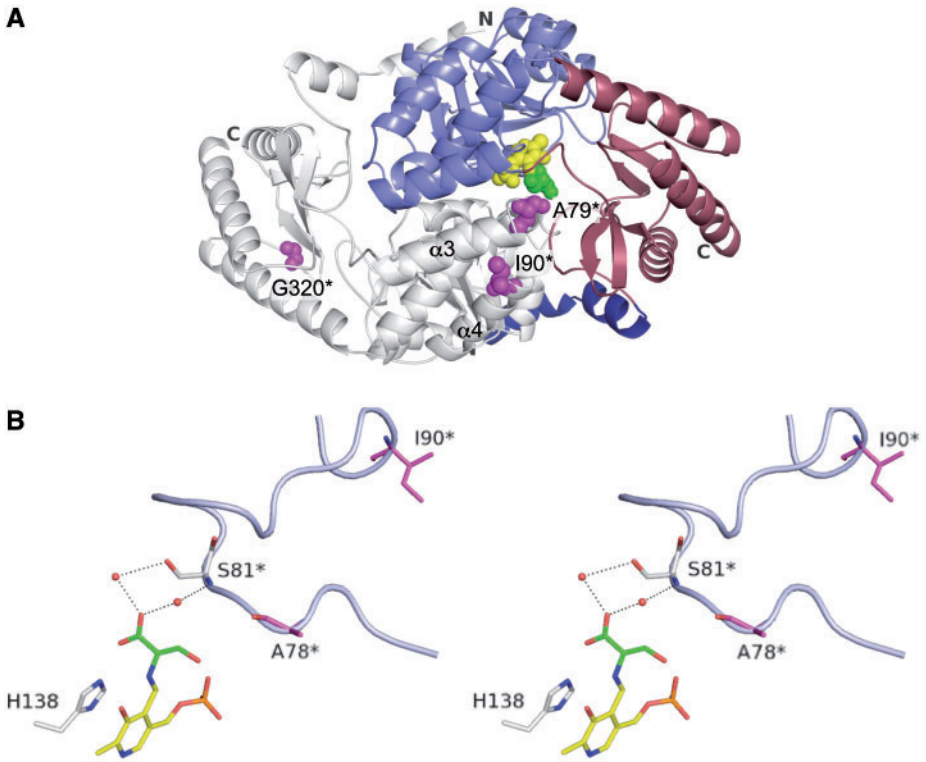

Fig. 7. **Location of the HSN1-related mutations in the crystal structure of the L-serine–SPT external aldimine complex.** (A) The overall structure of the SPT symmetric dimer in a complex with L-serine is shown in *ribbon* diagram. The three structural domains of subunit A and subunit B are colored in the same way as Fig. 4. The PLP and L-serine in subunit A are shown as *yellow* and *green* space-fill models, respectively. The HSN1-mutation sites (Ala79, Ile90 and Gly320) in subunit B are shown as a *magenta* space-fill model. (B) Close-up drawing of the active site in a parallel stereo view. The peptide region of 75–95 carrying the HSN1-related mutation sites is shown as a loop. The PLP–L-serine aldimine, His138, Ile90*, Ser81*, and Ala79* are shown as a stick model coloured in the same way as (A). The figure was drawn using PyMOL v0.99 (DeLano Scientific).

aldimine and amino-acid residues in the SPT active site explain the substrate specificity of SPT. The amino-acid residues highly conserved among the bacterial and eukaryotic SPTs are located in the 3D structure of this enzyme, and it allowed us to speculate their possible roles in the SPT catalysis or in the SPT-related hereditary disease. The interaction between the Nε2 of His138 and the carboxylate of L-serine is the first structural evidence strongly supporting the reaction regulation mechanism we have proposed. Thus, His138 fixes the orientation of the PLP-substrate aldimine to be unfavorable for α-deprotonation when only L-serine binds to the enzyme, thereby protecting the aldimine intermediate from any unwanted side reaction, such as abortive transamination. We have previously proposed additional roles of His138 in the later steps of the SPT catalysis; His138 enhances the Claisen-type condensation and decarboxylation by functioning as an acid catalyst, and avoids formation of the quinonoid intermediate from the SPT–KDS complex. These proposals will be further confirmed by ongoing crystallographic and kinetic studies using a series of substrate (product) analogues designed to mimic the intermediates and SPT mutants.

While the article is in the review process, an interesting article appeared describing the external aldimine form of spSPT (*46*). The conformation of the PLP–L-serine aldimine of spSPT was essentially the same as that of smSPT described in this paper, further supporting our proposal on the stereochemical control of the reaction of SPT. The most striking difference between the structures of the two SPTS is the region from β12 to β13. While His138 is the only residue in smSPT that fixes the orientation of the PLP–L-serine external-aldimine, both His159 and Arg378 forms a hydrogen bond with the carboxylate of L-serine in spSPT.

ACKNOWLEDGEMENTS

The synchrotron-radiation experiments at SPring-8 (proposal No. 2003A0780-RL1-np) were performed with the approval of the Japan Synchrotron Radiation Research Institute (to A.O.). We thank Dr. D. Yamamoto of Osaka Medical College for the technical advice on the model building of SPT.

FUNDING

Grants-in-Aid for Scientific Research (Category C. No. 21570120 to H.H. and, No. 21570149 and No. 18570114 to H.I.) from the Japan Society for the

Promotion of Science; the Osaka Medical Research Foundation for Incurable Diseases (to H.I.).

CONFLICT OF INTEREST

None declared.

REFERENCES

1. Uchida, Y. and Holleran, W.M. (2008) Omega-O-acylceramide, a lipid essential for mammalian survival. *J. Dermatol. Sci.* **51**, 77–87
2. Futerman, A.H. and Hannun, Y.A. (2004) The complex life of simple sphingolipids. *EMBO Rep.* **5**, 777–782
3. Spiegel, S. and Milstien, S. (2003) Sphingosine-1-phosphate: an enigmatic signalling lipid. *Nat. Rev. Mol. Cell. Biol.* **4**, 397–407
4. Munro, S. (2003) Lipid rafts: elusive or illusive? *Cell* **115**, 377–388
5. Hanada, K. (2003) Serine palmitoyltransferase, a key enzyme of sphingolipid metabolism. *Biochim. Biophys. Acta* **1632**, 16–30
6. Pinto, W.J., Srinivasan, B., Shepherd, S., Schmidt, A., Dickson, R.C., and Lester, R.L. (1992) Sphingolipid long-chain-base auxotrophs of *Saccharomyces cerevisiae*: genetics, physiology, and a method for their selection. *J. Bacteriol.* **174**, 2565–2574
7. Buede, R., Rinker-Schaffer, C., Pinto, W.J., Lester, R.L., and Dickson, R.C. (1991) Cloning and characterization of *LCB1*, a *Saccharomyces* gene required for biosynthesis of the long-chain base component of sphingolipids. *J. Bacteriol.* **173**, 4325–4332
8. Nagiec, M.M., Baltisberger, J.A., Wells, G.B., Lester, R.L., and Dickson, R.C. (1994) The LCB2 gene of *Saccharomyces* and the related LCB1 gene encode subunits of serine palmitoyltransferase, the initial enzyme in sphingolipid synthesis. *Proc. Natl Acad. Sci. USA* **91**, 7899–7902
9. Nagiec, M.M., Lester, R.L., and Dickson, R.C. (1996) Sphingolipid synthesis: identification and characterization of mammalian cDNAs encoding the Lcb2 subunit of serine palmitoyltransferase. *Gene* **177**, 237–241
10. Weiss, B. and Stoffel, W. (1997) Human and murine serine-palmitoyl-CoA transferase—cloning, expression and characterization of the key enzyme in sphingolipid synthesis. *Eur. J. Biochem.* **249**, 239–247
11. Hanada, K., Hara, T., Nishijima, M., Kuge, O., Dickson, R.C., and Nagiec, M.M. (1997) A mammalian homolog of the yeast LCB1 encodes a component of serine palmitoyltransferase, the enzyme catalyzing the first step in sphingolipid synthesis. *J. Biol. Chem.* **272**, 32108–32114
12. Hornemann, T., Richard, S., Rutti, M.F., Wei, Y., and von Eckardstein, A. (2006) Cloning and initial characterization of a new subunit for mammalian serine-palmitoyltransferase. *J. Biol. Chem.* **281**, 37275–37281
13. Hornemann, T., Wei, Y., and von Eckardstein, A. (2007) Is the mammalian serine palmitoyltransferase a high-molecular-mass complex? *Biochem. J.* **405**, 157–164
14. Ikushiro, H., Hayashi, H., and Kagamiyama, H. (2000) Expression and purification of serine palmitoyltransferase in *Biochemistry and Molecular Biology of Vitamin B6 and PQQ-dependent Proteins* (Iriarte, A., Kagan, H.M., and Martinez-Carrion, M., eds), pp. 251–254, Birkhäuser, Basel, Switzerland
15. Ikushiro, H., Islam, M.M., Tojo, H., and Hayashi, H. (2007) Molecular characterization of membrane-associated soluble serine palmitoyltransferases from *Sphingobacterium multivorum* and *Bdellovibrio stolpii*. *J. Bacteriol.* **189**, 5749–5761
16. Ikushiro, H., Hayashi, H., and Kagamiyama, H. (2001) A water-soluble homodimeric serine palmitoyltransferase from *Sphingomonas paucimobilis* EY2395^T strain. Purification, characterization, cloning, and overproduction. *J. Biol. Chem.* **276**, 18249–18256
17. Ikushiro, H., Hayashi, H., and Kagamiyama, H. (2003) Bacterial serine palmitoyltransferase: a water-soluble homodimeric prototype of the eukaryotic enzyme. *Biochim. Biophys. Acta* **1647**, 116–120
18. Ikushiro, H., Hayashi, H., and Kagamiyama, H. (2004) Reactions of serine palmitoyltransferase with serine and molecular mechanisms of the actions of serine derivatives as inhibitors. *Biochemistry* **43**, 1082–1092
19. Ikushiro, H., Fujii, S., Shiraiwa, Y., and Hayashi, H. (2008) Acceleration of the substrate Cα deprotonation by an analogue of the second substrate palmitoyl-CoA in serine palmitoyltransferase. *J. Biol. Chem.* **283**, 7542–7553
20. Shiraiwa, Y., Ikushiro, H., and Hayashi, H. (2009) Multifunctional role of His159 in the catalytic reaction of serine palmitoyltransferase. *J. Biol. Chem.* **284**, 15487–15495
21. Laemmli, U.K. (1970) Cleavage of structural proteins during the assembly of the head of bacteriophage T4. *Nature* **227**, 680–685
22. Otwinowski, Z. and Minor, W. (1997) Processing of X-ray diffraction data collected in oscillation mode. *Methods Enzymol.* **276**, 307–326
23. Vagin, A. and Teplyakov, A. (1997) MOLREP: an automated program for molecular replacement. *J. Appl. Cryst.* **30**, 1022–1025
24. Bailey, S. (1994) The CCP4 suite - programs for protein crystallography. *Acta Crystallog. Sect. D* **50**, 760–763
25. Schmidt, A., Sivaraman, J., Li, Y., Larocque, R., Barbosa, J.A., Smith, C., Matte, A., Schrag, J.D., and Cygler, M. (2001) Three-dimensional structure of 2-amino-3-ketobutyrate CoA ligase from Escherichia coli complexed with a PLP-substrate intermediate: inferred reaction mechanism. *Biochemistry* **40**, 5151–5160
26. Sali, A. and Blundell, T.L. (1993) Comparative protein modelling by satisfaction of spatial restraints. *J. Mol. Biol.* **234**, 779–815
27. Brunger, A.T., Adams, P.D., Clore, G.M., DeLano, W.L., Gros, P., Grosse-Kunstleve, R.W., Jiang, J.S., Kuszewski, J., Nilges, M., Pannu, N.S., Read, R.J., Rice, L.M., Simonson, T., and Warren, G.L. (1998) Crystallography & NMR system: a new software suite for macromolecular structure determination. *Acta Crystallog. Sect. D* **54**, 905–921
28. McRee, D.E. (1999) XtalView/Xfit - a versatile program for manipulating atomic coordinates and electron density. *J. Struct. Biol.* **125**, 156–165
29. Laskowski, R.A., MacArthur, M.W., Moss, D.S., and Thornton, J.M. (1993) PROCHECK: a program to check the stereochemical quality of protein structures. *J. Appl. Cryst.* **26**, 283–291
30. Yard, B.A., Carter, L.G., Johnson, K.A., Overton, I.M., Dorward, M., Liu, H., McMahon, S.A., Oke, M., Puech, D., Barton, G.J., Naismith, J.H., and Campopiano, D.J. (2007) The structure of serine palmitoyltransferase; gateway to sphingolipid biosynthesis. *J. Mol. Biol.* **370**, 870–886
31. Astner, I., Schulze, J.O., van den Heuvel, J., Jahn, D., Schubert, W.D., and Heinz, D.W. (2005) Crystal structure of 5-aminolevulinate synthase, the first enzyme of heme biosynthesis, and its link to XLSA in humans. *EMBO J.* **24**, 3166–3177
32. Webster, S.P., Alexeev, D., Campopiano, D.J., Watt, R.M., Alexeeva, M., Sawyer, L., and Baxter, R.L. (2000) Mechanism of 8-amino-7-oxononanoate synthase: spectroscopic, kinetic, and crystallographic studies. *Biochemistry* **39**, 516–528
33. Jansonius, J.N. (1998) Structure, evolution and action of vitamin B6-dependent enzymes. *Curr. Opin. Struct. Biol.* **8**, 759–769

34. Mehta, P.K. and Christen, P. (2000) The molecular evolution of pyridoxal-5′-phosphate-dependent enzymes. *Adv. Enzymol. Relat. Areas Mol. Biol.* **74**, 129–184
35. Schneider, G., Kack, H., and Lindqvist, Y. (2000) The manifold of vitamin B6 dependent enzymes. *Structure* **8**, R1–R6
36. Eliot, A.C. and Kirsch, J.F. (2004) Pyridoxal phosphate enzymes: mechanistic, structural, and evolutionary considerations. *Annu. Rev. Biochem.* **73**, 383–415
37. Alexeev, D., Alexeeva, M., Baxter, R.L., Campopiano, D.J., Webster, S.P., and Sawyer, L. (1998) The crystal structure of 8-amino-7-oxononanoate synthase: a bacterial PLP-dependent, acyl-CoA-condensing enzyme. *J. Mol. Biol.* **284**, 401–419
38. Dunathan, H.C. (1966) Conformation and reaction specificity in pyridoxal phosphate enzymes. *Proc. Natl Acad. Sci. USA* **55**, 712–716
39. Hunter, G.A., Zhang, J., and Ferreira, G.C. (2007) Transient kinetic studies support refinements to the chemical and kinetic mechanisms of aminolevulinate synthase. *J.Biol.Chem.* **282**, 23025–23035
40. Bejaoui, K., Wu, C., Scheffler, M.D., Haan, G., Ashby, P., Wu, L., de Jong, P., and Brown, R.H. Jr. (2001) SPTLC1 is mutated in hereditary sensory neuropathy, type 1. *Nat. Genet.* **27**, 261–262
41. Dawkins, J.L., Hulme, D.J., Brahmbhatt, S.B., Auer-Grumbach, M., and Nicholson, G.A. (2001) Mutations in SPTLC1, encoding serine palmitoyltransferase, long chain base subunit-1, cause hereditary sensory neuropathy type I. *Nat. Genet.* **27**, 309–312
42. Verhoeven, K., Coen, K., De Vriendt, E., Jacobs, A., Van Gerwen, V., Smouts, I., Pou-Serradell, A., Martin, J.J., Timmerman, V., and De Jonghe, P. (2004) SPTLC1 mutation in twin sisters with hereditary sensory neuropathy type I. *Neurology* **62**, 1001–1002
43. Gable, K., Han, G., Monaghan, E., Bacikova, D., Natarajan, M., Williams, R., and Dunn, T.M. (2002) Mutations in the yeast LCB1 and LCB2 genes, including those corresponding to the hereditary sensory neuropathy type I mutations, dominantly inactivate serine palmitoyltransferase. *J. Biol. Chem.* **277**, 10194–1200
44. Bejaoui, K., Uchida, Y., Yasuda, S., Ho, M., Nishijima, M., Brown, R.H. Jr., Holleran, W.M., and Hanada, K. (2002) Hereditary sensory neuropathy type 1 mutations confer dominant negative effects on serine palmitoyltransferase, critical for sphingolipid synthesis. *J Clin Invest.* **110**, 1301–1308
45. McCampbell, A., Truong, D., Broom, D.C., Allchorne, A., Gable, K., Cutler, R.G., Mattson, M.P., Woolf, C.J., Frosch, M.P., Harmon, J.M., Dunn, T.M., and Brown, R.H. Jr. (2005) Mutant SPTLC1 dominantly inhibits serine palmitoyltransferase activity in vivo and confers an age-dependent neuropathy. *Hum. Mol. Genet.* **14**, 3507–3521
46. Raman, M.C., Johnson, K.A., Yard, B.A., Lowther, J., Carter, L.G., Naismith, J.H., and Campopiano, D.J. (2009) *J. Biol. Chem.* **284**, 17328–17339